The Meteoritical Society

Meteoritics & Planetary Science 1–19 (2013)
doi: 10.1111/maps.12138

Vesta's mineralogical composition as revealed by the visible and infrared spectrometer on Dawn

M. Cristina De SANCTIS[1*], Eleonora AMMANNITO[1], M. Teresa CAPRIA[1], Fabrizio CAPACCIONI[1], Jean-Philippe COMBE[2], Alessandro FRIGERI[1], Andrea LONGOBARDO[1], Gianfranco MAGNI[1], Simone MARCHI[1,3], Tom B. McCORD[2], Ernesto PALOMBA[1], Federico TOSI[1], Francesca ZAMBON[1], Francesco CARRARO[1], Sergio FONTE[1], Y. J. LI[4], Lucy A. McFADDEN[5], David W. MITTLEFEHLDT[6], Carle M. PIETERS[7], Ralf JAUMANN[8], Katrin STEPHAN[8], Carol A. RAYMOND[9], and Christopher T. RUSSELL[10]

[1]Istituto di Astrofisica e Planetologia Spaziali, INAF, Rome, Italy
[2]Bear Fight Institute, 22 Fiddler's Road, Box 667, Winthrop, Washington 98862, USA
[3]NASA Lunar Science Institute, Boulder, Colorado, USA
[4]Planetary Science Institute, 1700 E. Ft. Lowell Rd., Tucson, Arizona 85719, USA
[5]NASA, Goddard Space Flight Center, Greenbelt, Maryland 20771, USA
[6]Astromaterials Research Office, NASA Johnson Space Center, Houston, Texas 77058, USA
[7]Brown University, Providence, Rhode Island 02912, USA
[8]Institute of Planetary Research, DLR, Berlin 80302, Germany
[9]Jet Propulsion Laboratory, Pasadena, California 91109, USA
[10]Institute of Geophysics and Planetary Physics, University of California, Los Angeles, California 90095–1567, USA
[*]Corresponding author. E-mail: mariacristina.desanctis@iaps.inaf.it

(Received 12 December 2012; revision accepted 02 May 2013)

Abstract–The Dawn spacecraft mission has provided extensive new and detailed data on Vesta that confirm and strengthen the Vesta–howardite–eucrite–diogenite (HED) meteorite link and the concept that Vesta is differentiated, as derived from earlier telescopic observations. Here, we present results derived by newly calibrated spectra of Vesta. The comparison between data from the Dawn imaging spectrometer—VIR—and the different class of HED meteorites shows that average spectrum of Vesta resembles howardite spectra. Nevertheless, the Vesta spectra at high spatial resolution reveal variations in the distribution of HED-like mineralogies on the asteroid. The data have been used to derive HED distribution on Vesta, reported in Ammannito et al. (2013), and to compute the average Vestan spectra of the different HED lithologies, reported here. The spectra indicate that, not only are all the different HED lithologies present on Vesta, but also carbonaceous chondritic material, which constitutes the most abundant inclusion type found in howardites, is widespread. However, the hydration feature used to identify carbonaceous chondrite material varies significantly on Vesta, revealing different band shapes. The characteristic of these hydration features cannot be explained solely by infalling of carbonaceous chondrite meteorites and other possible origins must be considered. The relative proportion of HEDs on Vesta's surface is computed, and results show that most of the vestan surface is compatible with eucrite-rich howardites and/or cumulate or polymict eucrites. A very small percentage of surface is covered by diogenite, and basaltic eucrite terrains are relatively few compared with the abundance of basaltic eucrites in the HED suite. The largest abundance of diogenitic material is found in the Rheasilvia region, a deep basin, where it clearly occurs below a basaltic upper crust. However, diogenite is also found elsewhere; although the depth to diogenite is consistent with one magma ocean model, its lateral extent is not well constrained.

INTRODUCTION

Prior Studies of Vesta's Mineralogy

Vesta is unique among objects in the asteroid Main Belt. Visible and near-IR spectroscopy from Earth-based telescopes (McCord et al. [1970] and many subsequent articles, e.g., Feierberg et al. 1980; Gaffey 1997; Binzel et al. 1997) showed that the surface of Vesta exhibits absorption features indicative of basaltic minerals, similar in composition to the howardite–eucrite–diogenite (HED) family of basaltic achondrite meteorites. This indicated that Vesta must have been molten and probably differentiated. NASA's Dawn spacecraft observed Vesta from orbit for slightly more than a year (Russell et al. 2012) with a suite of three instruments: a visible and infrared spectrometer—VIR (De Sanctis et al. 2011a), two redundant Framing Cameras—FC (Sierks et al. 2011), and a gamma ray and neutron detector—GRaND (Prettyman et al. 2012). The Dawn spacecraft permitted detailed study of Vesta's basaltic surface by VIR (De Sanctis et al. 2012), and together with the other instruments, confirmed that Vesta has experienced planetary-scale differentiation that produced a crust, mantle, and a core (Russell et al. 2012). Our knowledge of Vesta has been vastly increased by Dawn's brief stay.

Prior to Dawn's arrival in 2011, all information about Vesta was derived from telescopic observations, and inferred from the HED meteorites and theoretical modeling. High-quality reflectance spectra of Vesta acquired using Earth-based telescopes are available, owing to Vesta's location in the inner solar system, and its high albedo (infrared astronomical satellite [IRAS] albedo approximately 0.4) and relatively large size. Ground-based and HST images of Vesta revealed that the surface is not uniform, but instead exhibits local color and albedo variations of 10–20% (e.g., Binzel et al. 1997; Gaffey 1997; Thomas et al. 1997; Li et al. 2010). From Earth-based telescopes, only regional to hemispheric surface variations can be evaluated as the asteroid rotates. Gaffey (1997) observed subhemispheric color and spectral variations across the surface of Vesta, interpreting these differences as regions with differing mineralogies (eucrite-rich or diogenite-rich surface units, plus a possible olivine-rich region). According to Vernazza et al. (2005), the near-infrared spectra of Vesta show a surface composition closer to diogenites than eucrites and lower olivine contents than those obtained by Gaffey (1997). These remote observations were interpreted in different ways in terms of the types and distributions of the different minerals. The pyroxene mineral mapping from Dawn's orbit (De Sanctis et al. 2012a) finally yielded the precise locations of the diogenite-rich and eucrite-rich regions, providing regional and local geologic context for Vesta's HED lithologies.

These igneous rocks were apparently formed under reducing and volatile-poor conditions and suggest that Vesta has an anhydrous surface. However, previous ground-based observations reported different results on the presence of a 2.8 μm band on Vesta. Hasegawa et al. (2003) reported hydrated and/or hydroxylated minerals on the surface of part of the high albedo hemisphere of Vesta, whereas Rivkin et al. (2006) reported a small variation in the 2.95/2.20 μm band ratio, but found no conclusive evidence for the presence of hydrated materials on Vesta. Thus, the ground-based observations of Vesta in the spectral region of OH bands were not conclusive.

Visible and infrared spectrometer observations reported an absorption feature at 2.8 μm in some areas on Vesta (De Sanctis et al. 2012b). The 2.8 μm OH absorption band is unevenly distributed across Vesta's surface, indicating areas both rich and poor in hydrated materials. The hydration signature is primarily associated with dark material on Vesta and the origin of most of the OH is probably related to contamination of Vestan primordial material due to OH-bearing, low-velocity impactors (De Sanctis et al. 2012b; McCord et al. 2012). Further evidence of volatiles on Vesta is provided by the measurement of H in unidentified molecular form (Prettyman et al. 2012) and the existence of pitted terrains, interpreted as areas where volatiles were lost (Denevi et al. 2012).

Vesta and Vestoids

For a long time, Vesta was the only known asteroid having a basaltic crust (McCord et al. 1970; Larson and Fink 1975; McFadden et al. 1977; Binzel et al. 1997; Gaffey 1997), but in recent years, an increasing number of small asteroids with a similar surface composition have been discovered. These objects, taxonomically classified as V-type asteroids, pose a problem regarding the origin of basaltic material in the asteroid Main Belt. Most of them can be directly linked to Vesta, forming its dynamical family (the so-called Vestoids), but a few others do not appear to have a clear dynamical link to Vesta, suggesting the existence of other basaltic parent bodies. In particular, the discovery of small basaltic asteroids in the outer and intermediate Main Belt (Lazzaro et al. 2000), as well as in the inner belt, but far away from the dynamical limits of the Vesta family (Xu et al. 1995; Duffard et al. 2004; Alvarez-Candal et al. 2006), suggests the possibility that multiple differentiated parent bodies could have formed.

A strong indication of the presence of multiple basaltic asteroids, at least in the early phases of our

solar system, arises from diverse studies of these meteorites. Petrologic and compositional studies suggested that meteoritic basalts represent a minimum of five differentiated asteroids (Mittlefehldt 2005). Oxygen isotopic composition measurements suggest that although most HEDs are from the same parent body, four to six of them have values which are incompatible with a single origin for all HEDs (Greenwood et al. 2005; Scott et al. 2009). In addition, searches for meteorites in Antarctica resulting in new types of differentiated meteorites such as GRA 06128 and 06129 (Treiman et al. 2008) indicate that multiple differentiated planetesimals existed in the early solar system. Moreover, the abundance of iron meteorites having distinct elemental abundances argues for the existence of many differentiated bodies now disrupted. Therefore, there should be many potential leftovers of basaltic asteroids in the Main Belt.

The link between Vesta and Vestoids was reinforced by Hubble Space Telescope (HST) observations that discovered a large south polar basin (Thomas et al. 1997). The impact that formed this basin, now named Rheasilvia, is thought to have produced the Vestoids in orbits between Vesta and the 3:1 Jovian and v6 secular resonances (Binzel and Xu 1993; Marzari et al. 1996). The Vestoids are thought to be the immediate parent objects for most HED meteorites, thanks to the roles of the resonances that act as escape hatches from the Main Belt and provide trajectories into the inner solar system. Indeed, the reflectance spectra of Vesta (McCord et al. 1970; Gaffey 1997) and of Vestoids (Binzel and Xu 1993; Hiroi et al. 1995; Burbine et al. 2001; Duffard et al. 2004; Vernazza et al. 2005; Moskovitz et al. 2010; De Sanctis et al. 2011b, 2011c; Mayne et al. 2011) are very similar to those of HEDs, providing a further link with Vesta. The spectral data of Vestoids indicate varied mineralogy among these objects, ranging from diogenite-rich bodies to howardite-rich and eucritic-rich asteroids. The observed differences suggest that the spectral diversity observed among the Vestoids arises because these asteroids contain materials present on the Vesta surface or coming from different layers of Vesta excavated by collisions and not because they originated from different parent bodies (De Sanctis et al. 2011b, 2011c). Moreover, De Sanctis et al. (2011c) predicted a predominance of howardite–like mineralogy on Vesta's surface because most of the Vestoids are similar to howardite. These hypotheses are confirmed by Dawn spectral observations across Vesta's surface (De Sanctis et al. 2012a).

Vesta–HED Connection

The HEDs (see McSween et al. 2011) are a suite of basaltic and ultramafic meteorites, most of which come from Vesta (Russell et al. 2012). The first link between Vesta and HEDs is found in McCord et al. (1970) and Consolmagno and Drake (1977). The chronology of these samples indicates that the formation of Vesta's crust and mantle occurred in the first few million years of solar system history, well before larger terrestrial planets formed (Nyquist et al. 2003; Coradini et al. 2011a; Schiller et al. 2011). The complex Vestan surface and its collisional history (Keil 2002; De Sanctis et al. 2012a; Jaumann et al. 2012; Marchi et al. 2012) indicate that Vesta can thus be considered a proto-planet that was heated and differentiated early in solar system history, but somehow escaped being accreted into the terrestrial planets. Comprehensive reviews of the petrology, geochemistry, and geochronology of the HEDs can be found in Keil (2002) and McSween et al. (2011). The characteristics of HEDs that link them to Vesta are described in McSween et al. (2013b).

DAWN AT VESTA

Dawn's instrument suite was designed to characterize several aspects of Vesta's physical properties and composition. Visible and near-IR reflectance spectroscopy is the principal technique for asteroid surface mineralogical characterization. The nature of the solid compounds of the asteroid (silicates and oxides, plus organics and ices if they exist) can be identified by visual and infrared spectroscopy using high spatial resolution imaging to map the heterogeneity of asteroid surfaces and high spectral resolution to determine the composition unambiguously. The range of spatial information obtained by each instrument provides the essential geologic context needed to understand processes that occurred during Vesta's early evolution. Hyperspectral images in the visible and infrared regions reveal information on the mineralogical composition of the asteroid's surface.

Dawn was planned as a mapping mission and the mapping program was devised to take advantage of the steadily increasing spatial resolution provided by Dawn's three orbital phases: a Survey orbit at approximately 2700 km altitude (FC resolution of 260 m per pixel, VIR nominal resolution of 700 m per pixel), high altitude mapping orbit (HAMO) at 685 km altitude (FC resolution of 70 m per pixel, VIR nominal resolution of 200 m per pixel), and a low altitude mapping orbit (LAMO) at 200 km altitude (FC resolution of 20–25 m per pixel, VIR nominal resolution of 70 m per pixel). The HAMO orbits were performed in two different periods: HAMO-1 in autumn 2001 between Survey and LAMO, and HAMO-2 in early summer 2012 after LAMO. Dawn arrived at Vesta during the southern summer, thus allowing a complete

survey of the south polar region, and departed in August 2012, permitting the study of the northern regions, but in low illumination conditions.

VIR Instrument

The Visible and Infrared Spectrometer (VIR) instrument (De Sanctis et al. 2011a) measured reflectance spectra between 0.25 and 5.1 μm, a range that contains diagnostic mafic mineral absorption bands as well as the 3 μm "water" region. The VIR experiment aboard the Dawn mission is an advanced imaging spectrometer for planetary studies. It is derived from VIRTIS-M aboard Rosetta and Venus Express (Reininger et al. 1996; Coradini et al. 1998; Ammannito et al. 2006); all of these instruments are based on the optical layout introduced for the first time in Cassini/VIMS-V (Brown et al. 2005). VIR shares a Shafer telescope and an Offner relay between two spectral channels: the VIS channel operates in the 0.25–1.05 μm range, while the IR between 1.0 and 5.0 μm. The high spatial (IFOV = 250 μrad per pixel, FOV = 64 × 64 mrad) and spectral (ΔλVIS = 1.8 nm per band; ΔλIR = 9.8 nm per band) performances allow for the identification and mapping of the compositional units of the surfaces.

Using a scanning mirror, the scene is scanned one line at a time through the entrance slit of the spectrometer. Each line is made up of several pixels, each having a spectrum in the overall 0.25–5.1 μm range. The set of adjacent images is then stacked to form a "cube." In this way, one can extract a spectrum from each pixel (spatial location) in the data cube, showing the intensity of light as a function of the wavelength for that specific location. Alternatively, one can extract monochromatic images of the entire scene for a specific wavelength.

Visible and infrared spectrometers' excellent imaging capability combined with a broad spectral range gives us a geological context for mineralogy: spectra and derived spectral parameters can be mapped on Vesta with a resolution never achieved before. The derived lithological maps are described by Ammannito et al. (2013); here, we focus on the details of the spectra and of the derived spectral parameters for different Vestan terrains.

VIR Observations and Data Reduction

VIR acquired data of Vesta during all of the mission phases, from approach (May 2011) until departure (August 2012), for a total of more than one year of operations. The total number of spectra collected at Vesta, sampled in 864 spectral channels from 0.25 to 5.1 μm, exceeded 20 million, with variable spatial resolutions. Vesta was mapped with increasing spatial resolution from Survey orbits to LAMO orbits, but this increase was at the expense of the coverage. During Survey, 67% of Vesta's surface was acquired with a nominal resolution of 700 m, while during LAMO, only a few percent of the surface was covered with a nominal resolution of 70 m. Table 1 reports a summary of the data acquired during the different mission phases.

Table 1. Summary of the characteristics of the VIR data acquired during the orbital phases at Vesta.

	Survey	High altitude mapping orbit (1 + 2)	Low altitude mapping orbit
No. spectra	3.441.920	13.981.184	2.674.240
Gb	5.85	23.98	4.54
Nominal resolution	700 m	200 m	70 m

The data were calibrated and processed to analyze them in terms of overall Vesta mineralogy. The calibration file has been improved with respect to the data published in De Sanctis et al. (2012a) where a calibration artifact was present in the region between 2.5 and 3 μm. For the analysis of the 2.5 and 3 μm region, the following approach was adopted: VIR spectra were calibrated into bidirectional reflectance, with an incidence angle of 30° and an emergence angle of 0°. This calibration includes an empirical calibration of a global average of VIR spectra with a telescopic spectrum by Hasegawa et al. (2003). The purpose is only to remove systematic artifacts, but not to scale VIR spectra (De Sanctis et al. 2012a). The technique used is improved with respect to the spectra presented in De Sanctis et al. (2012b). Photometric effects are corrected for both topographic variations (Akimov disk function) and physical characteristics of the regolith (phase function model by Shkuratov et al. 1999).

The main spectral parameters derived are band centers, band depths, band areas, FWHM, asymmetry, spectral slopes, etc. The method used is the following: (1) Smoothing of the spectra with a boxcar average of three adjacent spectral channels; (2) evaluation of the spectral continuum, computed as a straight line between the relative maxima, and continuum removal; (3) evaluation of the band centers using a polynomial fit around the band minima (the band center being defined as the wavelength that corresponds to the minimum of the second-order polynomial fit around the minima of spectra); (4) evaluation of band depths that are defined as: 1-Rc/Rb, where Rb is the reflectance at the band minimum and Rc is the reflectance of the continuum at

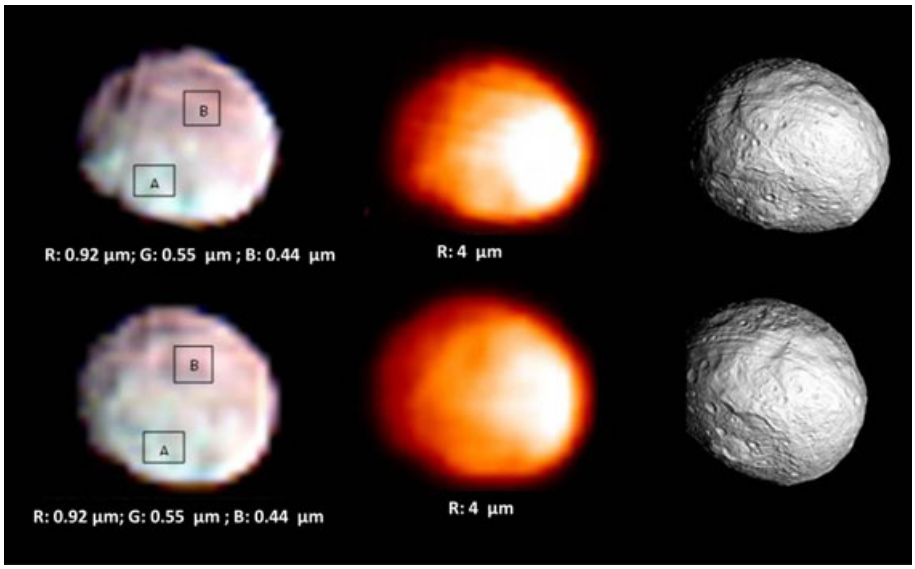

Fig. 1. Left panel: two Visible and Infrared Spectrometer (VIR) color composite images (red = 0.92 μm, green = 0.65 μm, blue = 0.44 μm). Central panel: two VIR false color images at 4 μm. Right panel: Vesta shape models showing the asteroid at the time of the observations. Spatial resolution is approximately 25 km per pixel.

the same wavelength as Rb. The details on the band parameters computation and the errors are given in Ammannito et al. (2013). Here, we describe the results obtained analyzing the spectra of different kinds of material present on Vesta as well as the average Vestan material.

VESTA SPECTRAL CHARACTERISTICS

Vesta Global Spectra

VIR spectra of Vesta's surface show ubiquitous absorption bands centered at approximately 0.9 and 1.9 μm, confirming the widespread occurrence of iron-bearing low-calcium pyroxenes (De Sanctis et al. 2012a). The first VIR spectra of Vesta with a resolution (approximately 25 km per pixel) better than Hubble data were acquired during the Approach phase, on June 30, 2011 (Fig. 1). Subspacecraft points for the two views of Vesta are located, respectively, at Lat. −31.96°, Lon. 126.57°, and Lat. −31.99°, Lon. 90.66°, (in Claudia prime meridian coordinate system) and were acquired about half an hour from each other.

The data used in this analysis have been improved with a new calibration that allowed removal of some artifacts present in the previous published data, in particular around 3 μm. The newly calibrated color composite image of Vesta (Fig. 1) demonstrates that there are large-scale variations in the spectral properties of the surface material, in particular between the southern hemisphere, where the large impact basin Rheasilvia is located, and the equatorial and northern regions. The average spectra from equatorial and southern regions are plotted in Fig. 2: the spectra show evidence of pyroxene absorption bands at 0.9 and 1.9 μm (hereafter, BI and BII, respectively). Longward of approximately 3.5 μm, the thermal emission of the surface dominates the spectra, and the spectral variations also reflect the local time with the corresponding surface temperature changes, as represented in Fig. 1 central panel, where the thermal emission at 4 μm is represented. Here, we will focus on the discussion on the spectral behaviors shortward of 3.5 μm: the thermal properties of Vesta are the subject of other studies.

The equatorial/northern region (reddish in Fig. 1, left panels) are characterized by shallower pyroxene absorption bands (Fig. 2) compared with the southern hemisphere (bluish in Fig. 1, left panels). The two pyroxene bands display distinct characteristics, being deeper and wider (larger band areas) in the South Polar region compared with the equatorial region (De Sanctis et al. 2012a). Moreover, the pyroxenes' band centers are displaced: the northern/equatorial regions have band centers at longer wavelengths (average BI = 0.930 μm and BII = 1.96 μm) compared with the south polar regions (average BI = 0.926 μm and BII = 1.94 μm). The different HED lithologies can be distinguished using pyroxene band centers' positions, although there is some overlap between howardites and the other lithologies, reflecting different mixing ratios.

Since these first data, Vesta shows clearer variation in mineralogy across its surface, with a special behavior

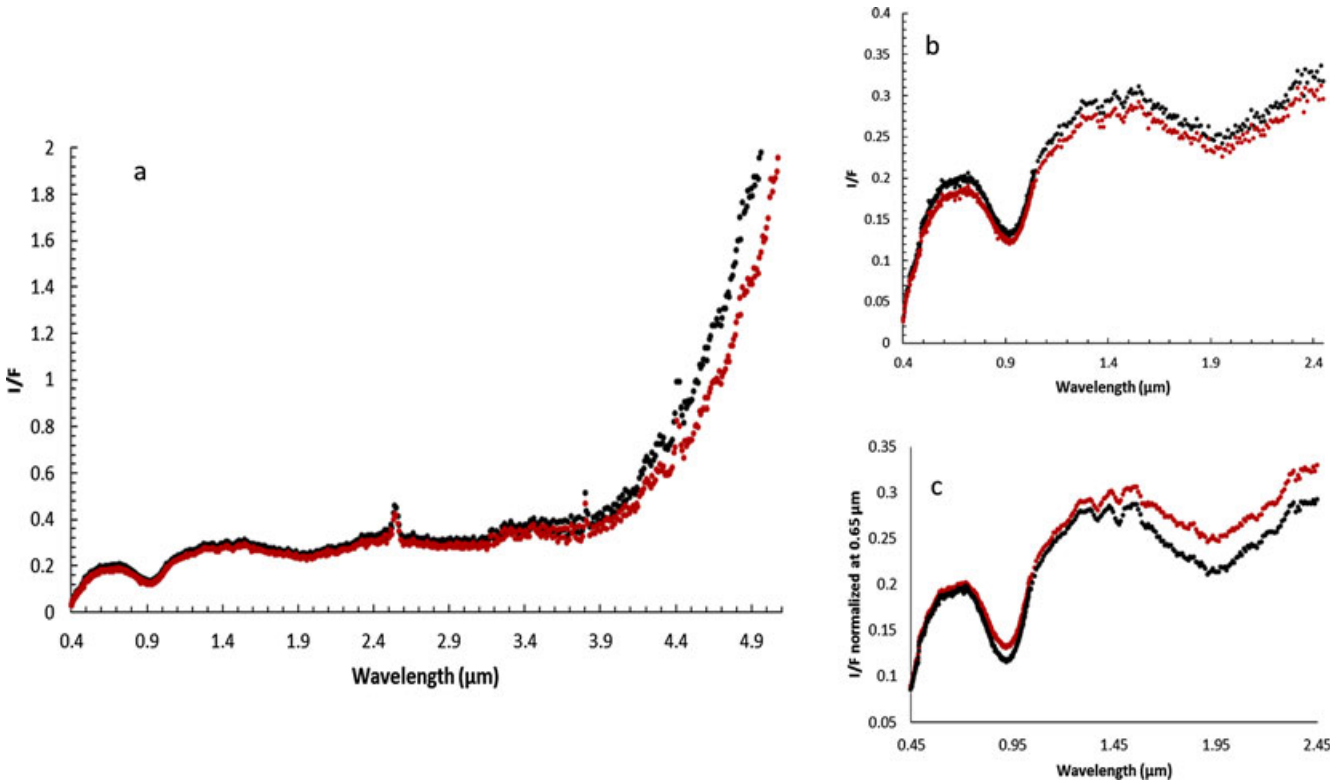

Fig. 2. a) Spectra of regions A and B as indicated in the VIR Vesta image in Fig. 1. Black: Vesta spectra taken from region A (southern); Red: Vesta spectra taken from region B (equatorial). The data between 2.48 and 2.58 μm and the data between 3.2 and 3.5 micron are affected by instrumental artifact. The region beyond 3.5 μm is dominated by the thermal emission from the surface. b) Spectra of regions A and B as indicated in the VIR Vesta image in Fig. 1. c) Normalized spectra of regions A and B; the spectra have been normalized at 0.65 μm to see the differences in band depth and shape.

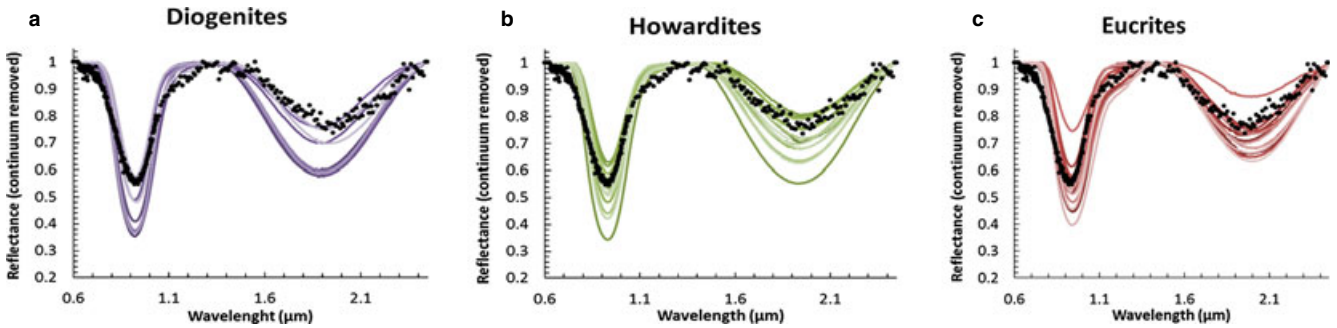

Fig. 3. a) Black: average Vesta spectrum, purple: laboratory spectra of diogenites. b) Black: average Vesta spectrum, green: laboratory spectra of howardites. c) Black: average Vesta spectrum, red: laboratory spectra of eucrites. The howardite-eucrite-diogenite data are from the RELAB database and are reported in Table 2.

of Rheasilvia basin (De Sanctis et al. 2012a; McSween et al. 2013), indicating that the composition and abundance of pyroxene in Rheasilvia are different. The spectra from the deeply excavated terrains in Rheasilvia have the characteristics of diogenitic material that clearly occurs below a basaltic upper crust.

The comparison between the average spectrum of Vesta taken from the data in Fig. 1 and HED spectra is in Fig. 3. The HEDs list is provided in Table 2. From Fig. 3, it is clear that Vesta spectra, on average, resemble those of howardites (breccia of eucrites and diogenites) in terms of the overall shape as well as band center positions, indicating a surface highly reworked and well mixed. However, a large spectral variability appears at increased spatial resolution (De Sanctis et al. 2012a). Some minor spectral differences may be attributed to alterations due to space weathering, rather than composition, as for some of the bright areas

Table 2. Band centers for diogenites, howardites, basaltic eucrites, polymitic, and cumulate eucrites. Band I and Band II centers have been computed using the method described above. The same method was also applied to VIR data of Vesta. The HED spectra were all taken at 0.005 μm intervals for samples with grain sizes of less than 25 μm (NASA RELAB facility at Brown University).

Basaltic eucrites	BII center (μm)	BI center (μm)	Polymitic/cumulate eucrites	BII center (μm)	BI center (μm)	Howardite	BII center (μm)	BI center (μm)	Diogenite	BII center (μm)	BI center (μm)
A87272	1.980	0.941	A881819	1.965	0.931	Bununu	1.950	0.930	A881526*	1.905	0.919
Bereba	2.015	0.940	ALH 78132*	1.955	0.930	EET 83376*	1.961	0.935	ALH 77256*	1.905	0.920
Bouvante	2.005	0.945	Moore County	1.985	0.935	EET 87503	1.950	0.930	Aiounel-Atrouss	1.920	0.925
Cachari*	1.995	0.941	Serra de Mage	1.966	0.931	EET 87513*	1.965	0.935	EETA79002	1.900	0.918
EET 87542*	1.995	0.945	ALHA76005*	1.970	0.935	Frankfort	1.951	0.930	GRO 95555*	1.919	0.921
EET 90020*	2.005	0.940	EETA79005*	1.971	0.935	GRO 95535	1.960	0.929	Johnstown	1.895	0.915
GRO 95533	2.015	0.939	LEW 87004	1.969	0.934	Kapoeta	1.954	0.928	LAP 91900	1.915	0.919
Jonzac	2.004	0.940	Y74450	1.980	0.936	LeTeilleul	1.945	0.928	Y74013*	1.920	0.921
Juvinas	1.995	0.936	Y792769	2.010	0.940	Petersburg*	1.975	0.935	Y75032*	1.945	0.925
Millbillillie	2.005	0.935	ALH 85001	1.950	0.925	QUE 94200	1.930	0.925	Tatahouine	1.905	0.920
PCA 82502	2.010	0.940				Y7308	1.945	0.927			
Padvarninkai	2.035	0.949				Y790727*	1.955	0.929			
Pasamonte	2.001	0.938				Y791573*	1.941	0.928			
Stannern	2.005	0.942									
Y792510*	2.005	0.942									

*Indicates HED that can be affected by terrestrial weathering.

discussed in the sections below (Pieters et al. 2012). Space weathering on Vesta has been a matter of debate because Vesta is bright and is found to have strong absorption bands (Vernazza et al. 2006; Marchi et al. 2010). Space-weathering effects on spectral data are discussed in Pieters et al. (2012).

The compositional diversity of Vesta's surface is unlike the spectrally uniform surfaces of the smaller asteroids visited by spacecraft previously (Veverka et al. 2000; Abe et al. 2006; Coradini et al. 2011) and is consistent with the mineralogical diversity among HEDs. The data at higher spatial resolution confirm the presence of diogenites, howardites, and eucrites on Vesta, as demonstrated in the following sections. This firmly supports the link between Vesta and the HED meteorites (McCord et al. 1970; Consolmagno and Drake 1977; Russell et al. 2012; McSween et al. 2013), providing geologic context for these samples and increasing our confidence in using laboratory studies of these meteorites to further understand the formation and evolution of Vesta.

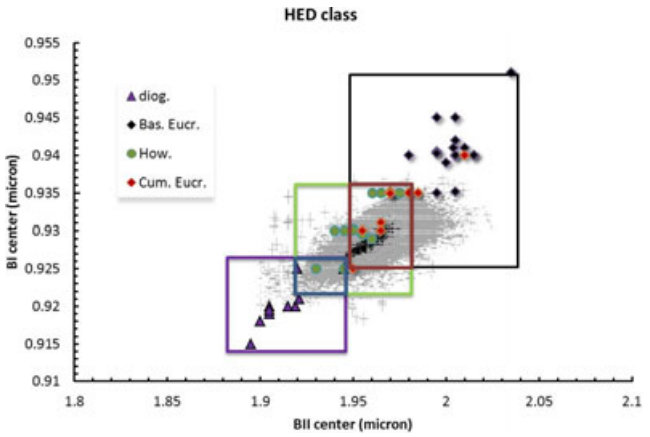

Fig. 4. Distribution of the band centers for the howardite-eucrite-diogenites listed in Table 2 and Vesta visible and infrared spectrometer (VIR) data. Purple, blue, green, red, and black boxes are the envelopes for diogenites, howardites/diogenites, howardites, eucrites/howardites, and eucrites, respectively. The gray points of the scatter plot represent the distribution of the VIR BI and BII centers acquired during the Survey phase.

Vesta Spectral Characteristics and Inferred Mineralogy

Pyroxenes are the most prominent spectral features on Vesta. Laboratory studies indicate that band centers for BI and BII pyroxene absorptions are systematically different for diogenites and eucrites (Gaffey 1976), so using a plot of BI versus BII centers, we can distinguish different lithologies on Vesta. To build a comparison database for Vesta, we perform the same spectral band analysis for each of the HED meteorites listed in Table 2 (Brown RELAB spectral catalog). We chose HED spectra corresponding to the smallest available grain size (for RELAB this is 25 μm), because it is believed that grains that compose the regolith of Vesta are very small (Hiroi et al. 1995). Some of these meteorites, marked with * in Table 2, could be affected by terrestrial weathering (Hiroi, personal communication) and their inclusion or exclusion in the plot slightly changes the overlapping region between the different HEDs. After a careful inspection of their spectra, we decided to include them in the plot, due to the lack of any clear sign of a 1.9 μm hydration band.

No temperature correction has been applied to the data. VIR observations are made at illumination conditions that maximize the S/N and, for this reason, the observations are acquired at similar local hours when the temperature is relatively high (approximately 250 K). Moreover, to compare observations obtained under similar conditions, we have filtered the data in such a way to avoid extreme conditions in terms of illumination angles and temperatures. The temperature effect on spectral parameters for the range of temperatures registered on Vesta during the VIR acquisitions here reported is negligible and within the errors of the band computation (Ammannito et al. 2013). Furthermore, due to the relatively high temperatures registered on Vesta during these acquisitions, the comparison with laboratory spectra taken at room temperature is appropriate.

A plot of BI center versus BII center for the HEDs is shown in Fig. 4. In this plot, diogenites and eucrites populate distinct areas because both BI and BII center positions are indicative of the different pyroxene compositions. BI and BII centers are at shorter wavelengths for diogenites than for eucrites, as a consequence of more Mg-rich pyroxenes with lower Ca concentrations in the former (Gaffey 1976; Cloutis et al. 1986). Howardites lie between and partially overlap the fields of diogenites and eucrites (Fig. 4). The eucrites can be further subdivided into cumulate/polymict eucrites and basaltic eucrites. The band centers of these two subgroups differ: cumulate eucrites plot in the lower part of the eucrite box and the basaltic eucrites lie mainly in the upper part. Unfortunately, the band centers of cumulate or polymict eucrites are indistinguishable from those of howardites making the identification of this lithology on Vesta very difficult based on the band centers (Fig. 4). The areas occupied by each subgroup have been outlined with different colors: purple for diogenite, green for howardite, black for eucrite, with overlapping fields of blue for diogenite–howardite and red for eucrite–howardite or cumulate eucrite (Fig. 4).

The derived distribution of BI versus BII centers in the Vesta spectra shows a trend from diogenites to

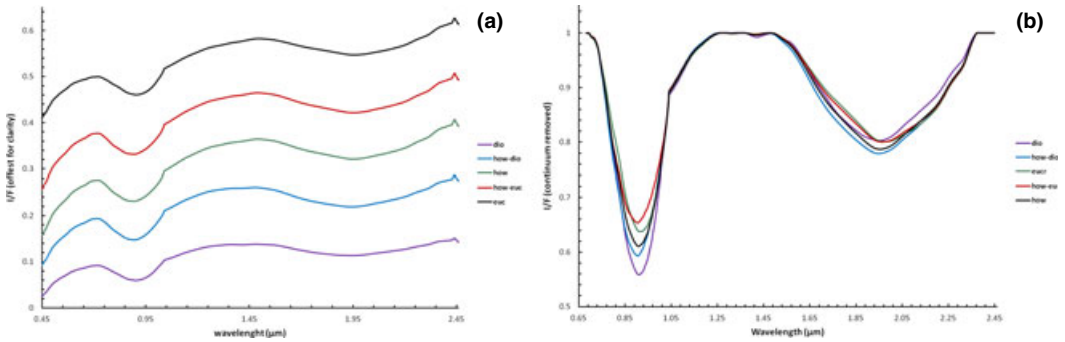

Fig. 5. a) Average spectra for each of the different classes depicted in Fig. 4. Purple, blue, green, red, and black spectra are the average of diogenites, howardites/diogenites, howardites, eucrites/howardites, and eucrites spectra, respectively; b) continuum removed spectra of Fig. 5a.

eucrites (Fig. 4, gray points). Most of the Vesta data acquired with VIR during Survey are compatible with eucrite-rich howardites and/or cumulate or polymict eucrites (red box). The boxes of the diogenites (purple) and the eucrites (black) are only partially filled. The most populated part of the Vestan eucrite box corresponds to the band center positions for cumulate or polymict eucrites, but their band centers are indistinguishable from howardites (Fig. 4). The basaltic eucrites box is not fully populated by Vestan data. Similarly, the diogenite box is not completely filled by VIR data. The explanation for this observation is not clear but, in this statistical approach, the plot is made using BI and BII values that occur at least ten times; as a consequence, the less frequent (and more extreme) values are discarded. Moreover, we note that not all the surface of Vesta has been mapped and the spatial resolution of the data used here is roughly 1 km. Thus, a possible explanation, beside the fact that "pure" diogenites may be so rare that they are not present, is that diogenites could occur in coherent areas smaller than the Survey pixel size. This is compatible with the relatively small proportion of diogenites on Vesta mapped by VIR (De Sanctis et al. 2012a; Ammannito et al. 2013; McSween et al. 2013): the Rheasilvia basin exposes diogenite at the base of its central uplift and in some places on the crater wall (McSween et al. 2013). Moreover, diogenites are the less represented group among HEDs in the U.S. Antarctic collection (McSween et al. 2013b), although they do make up approximately 20% of HEDS.

An analogous observational bias due to the statistical approach, the spatial resolution and the mapped regions, can be also proposed for the relatively small number of points in the basaltic eucrite region. When basaltic eucrite is mixed with cumulate eucrite or with diogenite, it becomes spectrally similar to cumulate eucrite or howardite. The mixing scale of the regolith on Vesta is likely the key to interpreting the observation that upper corner of the eucrite box is not populated.

Table 3. Average values of band centers of the different classes depicted in Fig. 5 derived from visible and infrared spectrometer Vestan data.

	BII center (μm)	BI center (μm)	STD BII center (μm)	STD BI center (μm)
Diogenites	1.908	0.922	0.014	0.002
Diogenites/ howardites	1.941	0.924	0.006	0.001
Eucrites	1.988	0.931	0.010	0.003
Howardites/ eucrites	1.969	0.930	0.006	0.002
Howardites	1.950	0.927	0.006	0.002

The most densely populated region in the scatter plot is the howardite area (green box) with a predominance of howardites enriched in eucrites (red box), suggesting that howardite constitutes the regolith of Vesta, or eucrites and diogenites occur within the regolith as blocks that are smaller than the spatial resolution for VIR maps. According to studies of the regolith thickness (Jaumann et al. 2012), the materials excavated by Rheasilvia would have incorporated various lithologies into the regolith, including igneous subsurface rocks.

Using the data of the scatter plot and the boxes indicative of the different mineralogies, we can associate each spectrum on Vesta with a particular lithology and compute the average spectrum representative of each of the described HED lithologies. The average spectrum of each HED lithology is shown in Fig. 5, where a progressive shift of the band centers to longer wavelengths in going from diogenites to eucrites is evident. The mean BI and BII centers with their standard deviations have also been computed for each class and are reported in Table 3.

The relative proportion of the different lithologies on Vesta's surface has been calculated using the data

Table 4. Percentage of Vesta's surface corresponding to howardite–eucrite–diogenites lithologies.

	Area (km^2)	Percentage relative to the total surface (%)	Percentage relative to the mapped surface (%)
Diogenites	1,162	0.1	0.2
Diogenites/ howardites	21,078	2.6	4.0
Eucrites	116,407	14.3	22.3
Howardites/ eucrites	345,429	42.4	66.3
Howardites	37,053	4.5	7.1
No coverage	294,199	36.0	—

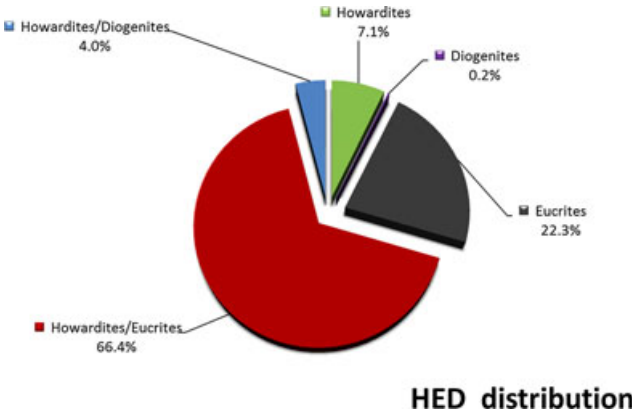

Fig. 6. Percentage of the different lithologies on the mapped part of Vesta's surface as revealed by visible and infrared spectrometer.

acquired during Survey orbits, when most of the asteroid was mapped. The percentages are relative to the total Vesta surface (approximately 815,000 km^2) in sinusoidal projection with a mean Vesta radius of 255 km (Table 4; Fig. 6). VIR, at the Survey resolution, reveals the preponderance of howardites rich in eucrites, indicating that eucritic lithology dominate, as they do among the HEDs. Diogenites are the less abundant class among HEDs and VIR spectral data confirm that they are the less represented lithology on Vesta. Hiroi et al. (1994) estimated the HED mixing ratios as diogenite 5–33%, eucrite 7–10%, and howardite 56–88%, with a large preponderance of howardites, similar to that found by VIR. McSween et al. (2013b) report the relative proportions of HED meteorites from Antarctica, where the preponderance of eucrites is evident. The comparison of these meteorite abundances with the Vestan surface lithologies is tricky for different reasons, including the fact that we could expect most of the material expelled from Rheasilvia comes from the upper crust and only a minor proportion from the lower crust/mantle.

The dominance of howardites indicates a strong gardening of the surface and a large degree of mixing, as also suggested by the kind of space weathering observed (Pieters et al. 2012). Regolith processes on Vesta produce a locally well-mixed surficial regolith. Small impacts continually stir the regolith, and this process is improved by regolith mobility due to Vesta's steep topography and local gravity gradients.

Although olivine is present in some diogenites (Beck and McSween 2010; Beck et al. 2011a), no clear spectral detections of olivine have yet been made in Rheasilvia. It must be recalled that it is difficult to spectrally distinguish olivine in concentrations <25% in the presence of abundant orthopyroxene (Beck et al. 2011b). Moreover, olivine-rich diogenites are relatively rare, suggesting that exposed olivine is not particularly abundant on Vesta's surface.

Bright and Dark Material

Bright materials on Vesta are distributed mainly in the equatorial region with two gaps, the first at Lon. 25°, 130°, Lat. −50°, 20° and the second at Lon. 200°, 280°, Lat. −70°, −20°. From the morphological analysis, it is possible to classify six different types of bright deposits: (1) Crater wall/scarp material (CWM), (2) Radial material (RM), (3) Spot material (SpM), (4) Slope material (SM), (5) Diffuse plains material (DPM), (6) Patchy material (PM) (Mittlefehldt et al. 2012). The albedo of the bright regions is much higher than the average of Vesta (i.e., 0.38). Compared with the surrounding areas, the CWM and SM are approximately 40% brighter, the RM is approximately 30–40% brighter; the bright spots are about 20–25% brighter; while the linear and patchy materials are about 20% brighter. Near the edge of the Rheasilvia basin, one crater includes some extremely bright areas with a geometric albedo of approximately 0.67 that is approximately 80% brighter than the Vestan average (Schroder et al. 2012).

An inventory of the bright-material deposits indicates that the most numerous types are CWM (≈46 deposits) and SM (≈46 deposits), followed by RM (≈19 deposits). A global overview of these deposits reveals that the largest concentrations of bright materials are located on the walls and/or in the ejecta of some large, morphologically young craters and this can be linked to their origin (McCord et al. 2012) and space weathering (Pieters et al. 2012). The fact that most of the bright deposits are concentrated in the large, young craters suggests that they are excavations of fresh material coming from underlying layers as a result of impacts. In

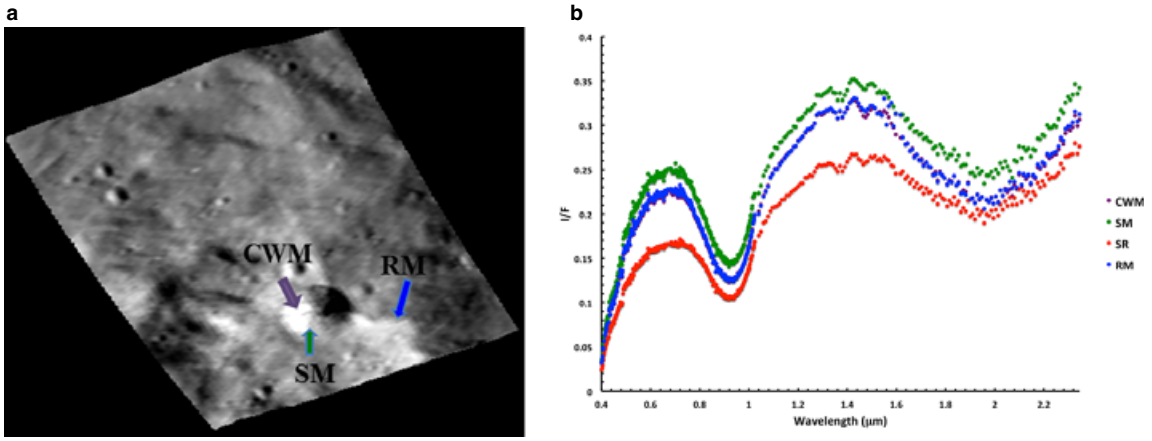

Fig. 7. a) VIR high altitude mapping orbit (HAMO) image of the Justina crater (−34°, 318°). The colored arrows indicate three different types of bright deposits present in this region: crater wall material (CWM)—purple, slope material (SM)—green, radial material (RM)—blue. b) Reflectance spectra of the regions annotated in Fig. 7a; crater wall material (CWM) in purple, slope material (SM) in green, radial material (RM) in blue, and surrounding material (SR) in red. The small bands around 1.4 μm are due to instrumental artifacts.

Fig. 7a, CWM deposits are recognizable as a high-reflectance lithologic unit below the surface, exposed by the falling material. In the same figures, the SM deposits are generated by the material coming from the bright lithologic unit (CWM). Representative spectra taken from the bright-material regions are plotted in Fig. 7b.

The derived band centers indicate that these deposits are representative of the different lithologies present on Vesta's surface. Some of them are mainly diogenite, while others are more consistent with howardite/eucrite. The band depth analysis shows that the bright deposits have deeper band depths than the surroundings areas. Deeper band depths could indicate a higher abundance of pyroxenes, but band depths are also affected by several factors, such as the grain size distribution and abundance of opaque materials, and it is not easy to distinguish a single contribution. Comparing the mean spectra of the three principal types of bright deposits (CWM, SM, RM), the CWM have deeper band depths than the other deposits. The SM and RM mean spectra are similar to each other and have similar band depths.

In Table 5, we report the average values of the photometrically corrected band depths obtained from the different bright deposits. The bright-material spectra show the classic strong pyroxene bands and the expected pyroxene continuum shape. The bright material is always associated with impacts and, therefore, the higher albedo and the stronger ferrous-iron absorption band of bright regions may indicate that this material belongs to a freshly exposed, unweathered Vestan lithology (Pieters et al. 2012). Considering this scenario, it is thus possible to exclude

Table 5. Mean value of the band depths I and II, photometrically corrected with an empirical method of the three principal types of bright materials compared with mean value of the band depths of the surrounding regions (SR).

	Crater wall/scarp material	Slope material	Radial material	SR
Band I depth	0.482	0.474	0.453	0.437
Band II depth	0.270	0.267	0.275	0.247

an exogenic origin of the bright deposits (McCord et al. 2012), but it is possible that bright material can be primordial Vesta basaltic soil, rich in unaltered, crystalline pyroxenes.

Dark materials are nonrandomly distributed on the Vestan surface and the albedo map exhibits broad low-albedo regions, especially between about 70° and 220° longitude, near which the localized dark material deposits (DMD) tend to cluster (Jaumann et al. 2012; McCord et al. 2012). Typically, the DMDs are associated with impact craters and are likely ejecta materials, both inside and outside craters. However, DMD can be associated with soil movements and mass wasting, too. All the dark deposits show the classical 1 and 2 μm pyroxene bands. The spectral differences among the DMDs, when present, are only subtle and suggest a composition similar to the Vestan average "material," with addition of a small amount of a moderate darkening agent. This agent is believed to have been produced mainly by exogenic sources: carbon-rich, low-velocity impactors deposited hydrated compounds onto the dark areas on Vesta, which show a

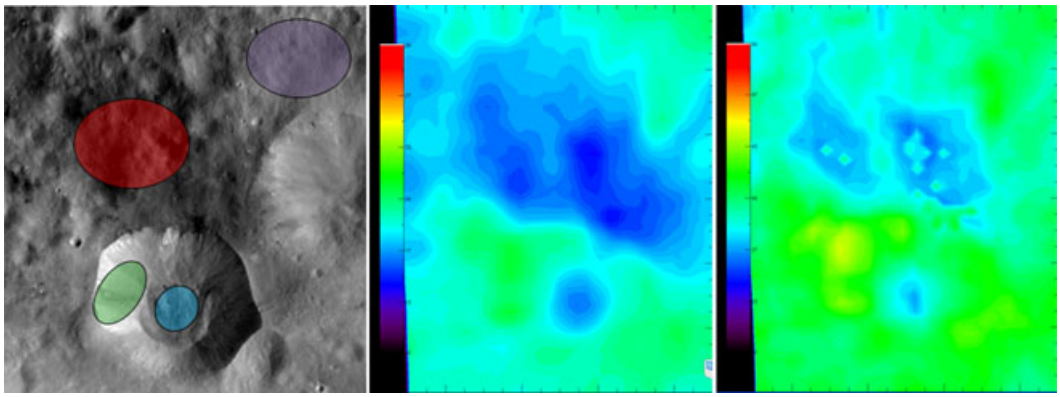

Fig. 8. Drusilla Crater seen by FC (left), the BI (center) and the BII (right) band depth distributions (bluer = weaker, yellow = stronger).

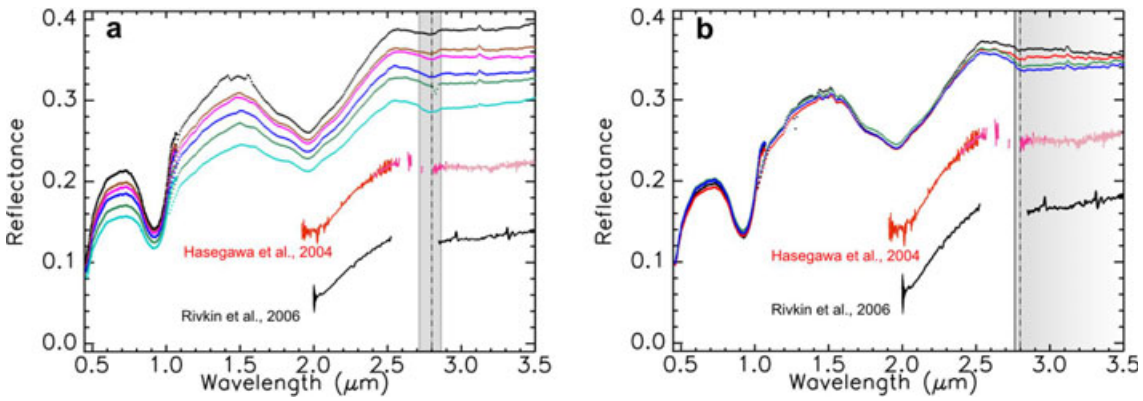

Fig. 9. Reflectance spectra of Vesta (after photometric correction) show various spectral features of hydrated minerals, indicated by the gray rectangles. Telescopic observations from Hasegawa et al. (2003) and Rivkin et al. (2006) are scaled and shifted for clarity; a) narrow, symmetric absorption, characteristic of vibration stretching mode between a cation from the host mineral and hydroxyl groups; b) broad asymmetric absorption observed West of Oppia crater, either due to OH- or H_2O-bearing phases.

weak but well-defined OH spectral feature at 2.8 μm (De Sanctis et al. 2012b; McCord et al. 2012). Freshly exposed mafic material or impact melt, created or exposed by impacts, both rich in opaque phases, are possible endogenic sources for the dark materials (McCord et al. 2012).

A complete study of the spectral parameters and behaviors of the DMD is under way and will be the subject of a forthcoming paper. A preliminary analysis shows a general slight decrease in both the BI and BII band depth of 10–20%, on average (Fig. 8). The most variable parameter is the BAR (band area ratio), which decreases as much as 50% relative to the Vestan average value (i.e., 1.8–2.0) in some dark deposits (Palomba et al. 2012). There are many examples of a large degree of spectral variation spatially inside a single deposit, suggesting that the darkening agent could be differentially mixed with the Vestan average regolith.

Hydrated Minerals

The surface of Vesta exhibits absorption features between 2.7 and 3.5 μm that are indicative of hydrated materials (De Sanctis et al. 2012b), as illustrated in Fig 9. Telescopic relative reflectance spectra by Hasegawa et al. (2003) and Rivkin et al. (2006) are shown for comparison of the shapes, but they are scaled and shifted, as they are not calibrated to absolute reflectance (Fig. 9). In all the examples presented in Fig. 9, the maximum absorption occurs at 2.81 μm, consistent with stretching vibrations of hydroxyl attached to a cation (M-OH). A similar absorption has been observed at the surface of the Moon (McCord et al. 2011). The position of this band depends in part on the nature of the cation (Farmer 1974; Sunshine et al. 2009). The shape of VIR spectra of the surface of Vesta between 2.7 and 3.5 μm (Fig. 9) is similar to

hydration features observed on the Moon (Clark 2009; Pieters et al. 2009; Sunshine et al. 2009), Mars (Jouglet et al. 2007; Milliken et al. 2007) and on C-Class asteroids (Rivkin et al. 2002). This complex feature can be attributed to asymmetric and symmetric stretching modes of the H_2O molecule or OH bonds that occur in this range of wavelengths.

Telescopic spectra from Hasegawa et al. (2003, 2004) and Rivkin et al. (2006) correspond to the average of the hemisphere that was facing the Earth at the time of the observation. Atmospheric water from the Earth absorbs most of the signal between 2.4 and 2.8 μm: the telescopic spectra shown in Fig. 9 have gaps in this spectral range. The spectrum by Hasegawa et al. restarts at 2.8 μm, at slightly shorter wavelength than the spectrum by Rivkin et al. (2006). Although the spectrum by Hasegawa et al. (2004) has been used as a reference for empirical calibration, individual VIR spectra show variations that reflect heterogeneity in composition across the surface of Vesta. Certain regions of Vesta have reflectance spectra without any absorption bands between 2.7 and 3.5 μm, which are consistent with the Rivkin et al. (2006) spectra. The short rise in the Hasegawa et al. (2004) spectrum beyond 2.8 μm is consistent with the narrow absorption band centered at 2.81 μm observed in VIR spectra.

Figure 9a shows a well-defined, narrow, and symmetric absorption band. As the depth of that absorption increases, the albedo decreases at all the wavelengths. At the global scale, the depth of the narrow absorption band at 2.8 μm shows a diffuse anticorrelation with albedo (De Sanctis et al. 2012b; McCord et al. 2012). This observation may indicate a possible common origin for hydrated minerals and dark materials. Infalling carbonaceous chondrite meteorites are candidates to explain this association as well as the distribution of these materials across the surface of Vesta (De Sanctis et al. 2012b; McCord et al. 2012).

A stronger 2.8 μm absorption band is also often associated with pyroxene bands at 1 and 2 μm shifted toward longer wavelengths, indicating basalts with relatively more calcium, as opposed to more magnesium. In the context of Vesta, more calcium in pyroxenes corresponds to eucrite. Eucrite-rich regions correspond to the older Vesta surface (Marchi et al. 2012); thus, the link between OH and eucrites-rich areas can be simply due to the old age of the latter allowing for greater accumulation of chondritic debris (De Sanctis et al. 2012b; Prettyman et al. 2012). In contrast, Fig. 9b shows VIR spectra with a shallow, broad and asymmetric absorption feature. The short-wavelength shoulder of that feature occurs at 2.76 μm (indicated by the left edge of the gray rectangle), and a sharp drop of reflectance rapidly reaches the local

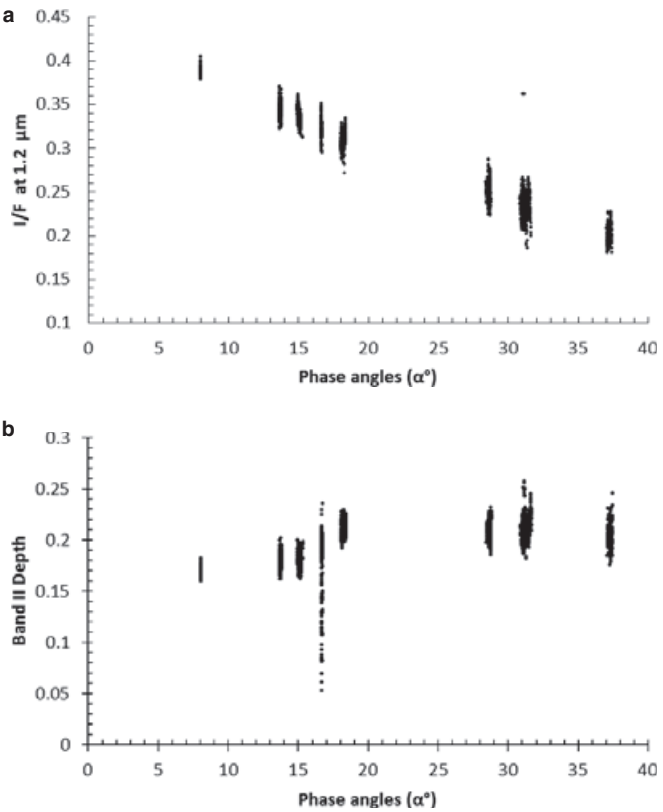

Fig. 10. a) I/F as function of phase angle. b) Band II depth as function of phase angle. The data are relative to observations of the 5° × 5° region, centered at 2.5°N, 303°E.

minimum at 2.8 μm (dash-dotted line). Past that local minimum toward the longer wavelength, reflectance increases very gradually, which makes the long-wavelength shoulder of that feature impossible to define (illustrated by the gradient of gray in the rectangle). This occurs when several absorption bands overlap each other (such as overtones). Four spectra collected in the ejecta blanket west of Oppia crater have similar albedo in the visible and near-infrared up to 2.5 μm, but the depth of the broad spectral hydration feature varies significantly. The complexity characteristic of this hydration feature combined with the relatively high albedo cannot be fully explained by infalling of carbonaceous chondrite meteorites. Other possible origins are under investigation.

Photometric Correction and Spectral Parameters

Calibrated VIR data show that I/F decreases with increasing phase angle (Fig. 10a). This is expected by the theoretical relationship between radiance and observation geometry (Hapke 1963, 1981). The reflectance also depends on local illumination and viewing angles, showing limb-to-terminator variations. This limb-to-terminator behavior depends on the

roughness of the surface as well as optical properties such as albedo and transparency. The geometry dependence of reflectance affects the spectral slopes and band characteristics, causing the so-called "phase reddening" effect. Ground-based observations of Vesta and laboratory measurements of HED meteorites show that the spectral slope and both band depths (Fig. 10b) increase with increasing phase angles until approximately 25º, then the band strength stays flat or slightly decreases with phase angle (Reddy et al. 2012). If not accounted for, the phase reddening will inevitably bias the interpretations of spectra.

To remove the dependence of reflectance on scattering geometry, a photometric model has been developed, based on the shape model of Vesta derived from Dawn FC images using a stereo imaging technique with Survey data (Jaumann et al. 2012). This is a 5-parameter Hapke model, where the opposition parameters B_0 and h are fixed at 1.03 and 0.04, respectively (Veverka et al. 1980), due to the lack of sufficient data at small phase angles to constrain the opposition effect. The single scattering albedo, the phase function parameter, and the macroscopic roughness are retrieved by a fit on VIR data (Li et al. 2012).

Band depth variations with phase are as high as 10–15% for Band I and 20–25% for Band II as shown in VIR data. These variations are consistent with the previous ground-based observations of Vesta and laboratory measurements of HED meteorites, and are similar to that observed on Eros (Bell et al. 2002). The photometric properties of the band depths of various surface regions can be studied in greater detail by taking into account the dependence on the phase angle, and on the incidence and emission angles. It is observed that bright regions show variation in the band depth with the incidence angle, but that they are almost independent of emission angle; the reverse is true for dark regions. This can be readily explained in terms of the relative importance of the multiple scattering with respect to single scattering in bright and dark regions. The interpretation of this effect is the subject of an upcoming paper.

SUMMARY

VIR spectra indicate that all the different HED lithologies are present on Vesta's surface and their distributions give the geologic context for these meteorites (Ammannito et al. 2013).

Using the BI/BII diagram, we can associate Vestan spectra with specific HED lithologies and it is possible to compute the percentage of Vesta surface that shows a specific lithology.

Following this approach, the dominant lithology exposed on Vesta is howardite-rich in eucrites. Although cumulate eucrites also match the spectral characteristics, they are of much lower abundance in the HED suite and are not a major component of howardites (McSween et al. 2011). Pure diogenites and basaltic eucrites are less represented, suggesting that they occur on the surface in regions that are smaller than the spatial resolution for VIR pixels, for example as blocks within the regolith. Large regions have spectral characteristics of eucrite material. In the BI/BII diagram, most of their band centers plot in the regions of cumulate or polymict eucrites, that is, coincident with the howardite-rich in eucrites area, while basaltic eucrites seem less represented on Vesta's surface, due to the paucity of band centers consistent with pure basaltic eucrites.

Eucrites are the predominant type among HEDs, while diogenites are the less abundant class. VIR spectral data confirm that they are the less represented lithology on Vesta. They occurs in small coherent areas mainly in the deeply excavated Rheasilvia basin (Ammannito et al. 2013; McSween et al. 2013).

Different models for diogenite formation have been suggested: (1) magma ocean models that predict a thick layer of cumulate diogenite below a basaltic crust (Righter and Drake 1997; Warren 1997) and (2) serial magmatism models that posit diogenite-bearing plutons near the crust-mantle boundary or within the lower crust (Mittlefehldt 1994; Shearer et al. 1997; Barrat et al. 2008; Beck and McSween 2010).

Diogenite is revealed by VIR, and its occurrence at the lowest levels on the Rheasilvia basin floor indicates that material of the lower crust/upper mantle was exposed. Moreover, an extensive ejecta blanket produced by the Rheasilvia-forming impact covers a broad portion of Vesta's surface (Ammannito et al. 2013). The spectra of the ejecta are consistent with those of howardites and indicate a regolith with varying proportions of eucrite and diogenite. In some places, the howarditic ejecta show a consistent component of diogenite. However, the diogenite distribution mapped so far does not give unambiguous constraints for any of the proposed formation models, even though the depth where diogenite-rich material is exposed could favor the hypothesis of magma ocean models.

Pyroxenes are ubiquitous on Vesta and there is no convincing spectral evidence for lithologies not already represented in HED meteorites. The strong pyroxene absorption bands typical of the bright materials indicate such material as intrinsic Vesta basaltic soil, rich in unaltered, crystalline pyroxenes.

Moreover, the spectra of some regions on Vesta reveal the presence of the most abundant type of

xenolith in howardites: carbonaceous chondrites. The spectra of the dark regions show an OH feature, consistent with the presence of hydrated carbonaceous chondrite in the most ancient regolith (De Sanctis et al. 2012b; McCord et al. 2012; Prettyman et al. 2012). However, VIR recognizes differences in the hydration band shapes that cannot be fully equated with the signature of carbonaceous chondrites.

Furthermore, the spectral data indicate that the "classical space-weathering" products of grain coatings of nanophase iron particles, common on the Moon and smaller asteroids, seem not to be present in any considerable amount on Vesta (Pieters et al. 2012). The bright material shows a systematic increase in band depths with respect to the surrounding materials, while the dark material shows an opposite trend, indicative of material "contaminated" by the addition of a moderate darkening agent.

The Dawn mission provides the first spatially resolved spectra of Vesta and offers a detailed view of the distribution of the rock types, reinforcing the link between Vesta and HED meteorites.

Acknowledgments—VIR is funded by the Italian Space Agency and was developed under the leadership of INAF-Istituto di Astrofisica e Planetologia Spaziali, Rome, Italy. The instrument was built by Selex-Galileo, Florence, Italy. The authors acknowledge the support of the Dawn Science, Instrument, and Operations Teams. We also acknowledge H. Y. McSween, T. Hiroi, and R. Binzel for their helpful comments. This work was supported by the Italian Space Agency and NASA's Dawn at Vesta Participating Scientists Program. A portion of this work was performed at the Jet Propulsion Laboratory under contract with NASA. This research utilizes spectra of the NASA RELAB facility at Brown University.

Editorial Handling—Dr. Hap McSween

REFERENCES

Abe M., Takagi Y., Kitazato K., Abe S., Hiroi T., Vilas F., Clark B. E., Abell P. A., Lederer S. M., Jarvis K. S., Nimura T., Ueda Y., and Fujiwara A. 2006. Near-infrared spectral results of asteroid Itokawa from the Hayabusa spacecraft. *Science* 312:1334–1338, doi:10.1126/science.1125718.

Alvarez-Candal A., Duffard R., Lazzaro D., and Michtchenko T. 2006. The inner region of the asteroid Main Belt: A spectroscopic and dynamic analysis. *Astronomy & Astrophysics* 459:969–976.

Ammannito E., Filacchione G., Coradini A., Capaccioni F., Piccioni G., De Sanctis M. C., Dami M., and Barbis A. 2006. On-ground characterization of Rosetta/VIRTIS-M. I. Spectral and geometrical calibrations. *Review of Scientific Instruments* 77:093109, doi:10.1063/1.2349308.

Ammannito E., De Sanctis M. C., Capaccioni F., Capria M. T., Carraro F., Combe J.-P., Fonte S., Frigeri A., Joy S., Longobardo A., Magni G., Marchi S., McCord T. B., McFadden L. A, McSween H. Y., Palomba E., Pieters C. M., Polanskye C. A., Raymond C. A., Sunshine J., Tosi F., Zambon F., and Russell C. T. 2013. Vestan lithologies mapped by VIR. *Meteoritics & Planetary Science* 48, doi:

Barrat J. A., Yamaguchi A., Benoit M., Cotton J., and Bohn M. 2008. Geochemistry of diogenites: Still more diversity in their parental melts. *Meteoritics & Planetary Science* 43:1759–1775.

Beck A. W. and McSween H. Y. 2010. Diogenites as polymict breccias composed of orthopyroxenite and harzburgite. *Meteoritics & Planetary Science* 45:850–872, doi:10.1111/j.1945-5100.2010.01061.x.

Beck A. W., Mittlefehldt D. W., McSween H. Y., Rumble D., Lee C.-T. A., and Bodnar R. J. 2011a. MIL 03443, a dunite from asteroid 4 Vesta: Evidence for its classification and cumulate origin. *Meteoritics & Planetary Science* 46:1133–1151, doi:10.1111/j.1945-5100.20111.01219.x.

Beck P., Barrat J.-A., Grisolle F., Quirico E., Schmitt B., Moynier F., Gillet P., and Beck C. 2011b. NIR spectral trends of HED meteorites: Can we discriminate between the magmatic evolution, mechanical mixing and observation geometry effects? *Icarus* 216:560–571, doi:10.1016/j.icarus.2011.09.015.

Bell J. F., Izenberg N. I., Lucey P. G., Clark B. E., Peterson C., Gaffey M. J., Joseph J., Carcich B., Harch A., Bel M. E., Warren J., Martin P. D., McFadden L. A., Wellnitz D., Murchie S., Winter M., Veverka J., Thomas P., Robinson M. S., Malin M., and Cheng A. 2002. Near-IR reflectance spectroscopy of 433 Eros from the NIS instrument on the NEAR Mission. I. Low phase angle observations. *Icarus* 155:119–144.

Binzel R. P. and Xu S. 1993. Chips off asteroid 4 Vesta: Evidence for the parent body of basaltic achondrite meteorites. *Science* 260:186–191.

Binzel R. P., Gaffey M. J., Thomas P. C., Zellner B. H., Storrs A. D., and Wells E. N. 1997. Geologic mapping of Vesta form 1994 Hubble Space Telescope images. *Icarus* 128:95–103.

Brown R. H., Baines K. H., Bellucci G., Bibring J. P., Buratti B. J., Capaccioni F., Cerroni P., Clark R. N., Coradini A., Cruikshank D. P., Drossart P., Formisano V., Jaumann R., Langevin Y., Matson D. L., McCord T. B., Mennella V., Miller E., Nelson R. M., Nicholson P. D., Sicardy B., and Sotin C. 2005. The Cassini visual and infrared mapping spectrometer (VIMS) investigation. *Space Science Reviews* 115:111–168.

Burbine T. H., Buchanan P. C., Binzel R. P., Bus S. J., Hiroi T., Hinrichs J. L., Meibom A., and McCoy T. J. 2001. Vesta, Vestoids, and the howardite, eucrite, diogenite group: Relationships and the origin of spectral differences. *Meteoritics & Planetary Science* 36:761–781.

Clark R. N. 2009. Detection of adsorbed water and hydroxyl on the Moon. *Science* 326:562–564, doi:10.1126/science.1178105.

Cloutis E. A., Gaffey M. J., Jackowski T. L., and Reed K. L. 1986. Calibrations of phase abundance, composition, and particle-size distribution for olivine-orthopyroxene mixtures from reflectance spectra. *Journal of Geophysical Research—Solid Earth Planets* 91:1641–1653.

Consolmagno G. J. and Drake M. J. 1977. Composition of the eucrite parent body: Evidence from rare Earth elements. *Geochimica et Cosmochimica Acta* 41:1271–1282.

Coradini A. Capaccioni F., Drossart P., Semery A., Arnold G., Schade U., Angrilli F., Barucci M. A., Bellucci G., Bianchini G., Bibring J. P., Blanco A., Blecka M., Bockelee-Morvan D., Bonsignori R., Bouye M., Bussoletti E, Capria M. T., Carlson R., Carsenty U., Cerroni P., Colangeli L., Combes M., Combi M., Crovisier J., Dami M., De Sanctis M. C., DiLellis A. M., Dotto E., Encrenaz T., Epifani E., Erard S., Espinasse S., Fave A., Federico C., Fink U., Fonti S., Formisano V., Hello Y., Hirsch H., Huntzinger G., Knoll R., Kouach D., Ip W. P., Irwin P., Kachlicki J., Langevin Y., Magni G., McCord T., Mennella V., Michaelis H., Mondello G., Mottola S., Neukum G., Orofino V., Orosei R., Palumbo P., Peter G., Pforte B., Piccioni G., Reess J. M., Ress E., Saggin B., Schmitt B., Stefanovitch D., Stern A., Taylor F., Tiphene D., and Tozzi G. 1998. VIRTIS: An imaging spectrometer for the ROSETTA mission. *Planetary and Space Science*. 46:1291–1304.

Coradini A., Turrini D., Federico C., and Magni G. 2011a. Vesta and Ceres: Crossing the history of the solar system. *Space Science Reviews* 163:25–40.

Coradini A., Capaccioni F., Erard S., Arnold G., De Sanctis M. C., Filacchione G., Tosi F., Barucci M. A., Capria M. T., Ammannito E., Grassi D., Piccioni G., Giuppi S., Bellucci G., Benkhoff J., Bibring J. P., Blanco A., Blecka M., Bockelee-Morvan D., Carraro F., Carlson R., Carsenty U., Cerroni P., Colangeli L., Combes M., Combi M., Crovisier J., Drossart P., Encrenaz E. T., Federico C., Fink U., Fonti S., Giacomini L., Ip W. H., Jaumann R., Kuehrt E., Langevin Y., Magni G., McCord T., Mennella V., Neukum G., Orofino V., Palumbo P., Schade U., Schmitt B., Taylor F., Tiphene D., and Tozzi G. 2011b. The surface composition and temperature of asteroid 21 Lutetia as observed by Rosetta/VIRTIS. *Science* 334:492–494.

De Sanctis M. C., Coradini A., Ammannito E., Filacchione G., Capria M. T., Fonte S., Magni G., Barbis A., Bini A., Dami M., Ficai-Veltroni I., and Preti G. 2011a. The VIR spectrometer. *Space Science Reviews* 163:329–369.

De Sanctis M. C., Migliorini A., Luzia Jasmin F., Lazzaro D., Filacchione G., Marchi S., and Ammannito E. 2011b. Spectral and mineralogical characterization of inner main-belt V-type asteroids. *Astronomy and Astrophysics* 533: A77, doi:10.1051/0004-6361/201117136.

De Sanctis M. C., Ammannito E., Migliorini A., Lazzaro D., Capria M. T., and McFadden L. 2011c. Mineralogical characterization of some V-type asteroids, in support of the NASA Dawn mission. *Monthly Notices of the Royal Astronomical Society* 412:2318–2332.

De Sanctis M. C., Ammannito E., Capria M. T., Tosi F., Capaccioni F., Zambon F., Carraro F., Fonte S., Frigeri A., Jaumann R., Magni G., Marchi S., McCord T. B., McFadden L. A., McSween H. Y., Mittlefehldt D. W., Nathues A., Palomba E., Pieters C. M., Raymond C. A., Russell C. T., Toplis M. J., and Turrini D. 2012a. Spectroscopic characterization of mineralogy and its diversity across Vesta. *Science* 336:697–700, doi:10.1126/science.1219270.

De Sanctis M. C., Combe J.-P., Ammannito E., Palomba E., Longobardo A., McCord T. B., Marchi S., Capaccioni F., Capria M. T., Mittlefehldt D. W., Pieters C. M., Sunshine J., Tosi F., Zambon F., Carraro F., Fonte S., Frigeri A., Magni G., Raymond C. A., Russell C. T., and Turrini D. 2012b. Detection of widespread hydrated materials on Vesta by VIR imaging spectrometer on board the Dawn mission. *The Astrophysical Journal Letters* 758:L36.

Denevi B. W., Blewett D. T., Buczkowski D. L., Capaccioni F., Capria M. T., De Sanctis M. C., Garry W. B., Gaskell R. W., Le Corre L., Li J.-Y., Marchi S., McCoy T. J., Nathues A., O'Brien D. P., Petro N. E., Pieters C. M., Preusker F., Raymond C. A., Reddy V., Russell C. T., Schenk P., Scully J. E. C., Sunshine J. M., Tosi F., Williams D. A., and Wyrick D. 2012. Pitted terrain on Vesta and implications for the presence of volatiles. *Science* 338:246–249, doi:10.1126/science.1225374.

Duffard R., Lazzaro D., Licandro J., De Sanctis M. C., Capria M. T., and Carvano J. M. 2004. Mineralogical characterization of some basaltic asteroids in the neighborhood of (4) Vesta: First results. *Icarus* 171:120–132.

Farmer V. C. 1974. *The infrared spectra of minerals*. London: Mineralogical Society, monograph 4.

Feierberg M. A., Larson H. P., Fink U., and Smith H. A. 1980. Spectroscopic evidence for two achondrit parent bodies: Asteroid 349 Dembowska and 4 Vesta. *Geochimica et Cosmochimica Acta* 44:513–524.

Gaffey M. J. 1976. Spectral reflectance characteristics of the meteorite classes. *Journal of Geophysical Research* 81:905–920.

Gaffey M. J. 1997. Surface lithologic heterogeneity of asteroid 4 Vesta. *Icarus* 127:130–157.

Greenwood R. C., Franchi I. A., Jambom A., and Buchanan P. 2005. Widespread magma oceans on asteroidal bodies in the early solar system. *Nature* 435:916–918.

Hapke B. 1963. A theoretical photometric function for the lunar surface. *Journal of Geophysical Research* 68:4571–4586.

Hapke B. 1981. Bidirectional reflectance spectroscopy. 1. Theory. *Journal of Geophysical Research* 86:4571–4586.

Hasegawa S., Murakawa K., Ishiguro M., Nonaka H., Takato N., Davis C. J., Ueno M., and Hiroi T. 2003. Evidence of hydrated and/or hydroxylated minerals on the surface of asteroid 4 Vesta. *Geophysical Research Letters* 30:2123–2126, doi:10.1029/2003GL018627.

Hasegawa S., Hiroi T., Ishiguro M., Nonaka H., Takato N., Davis C. J., Ueno M., and Murakawa K. 2004. Spectroscopic observations of asteroid 4 Vesta from 1.9 to 3.5 micron: Evidence of hydrated and/or hydroxylated minerals (abstract #1458). 35th Lunar and Planetary Science Conference. CD-ROM.

Hiroi T., Pieters C. M. and Takeda H. 1994. Grain size of the surface regolith of asteroid 4 Vesta estimated from its reflectance spectrum in comparison with HED meteorites. *Meteoritics* 29:394–396.

Hiroi T., Binzel R. P., Sunshine J. M., Pieters C. M., and Takeda H. 1995. Grain sizes and mineral compositions of surface Regoliths of Vesta-like asteroids. *Icarus* 115:374–386, doi:10.1006/icar.1995.1105.

Jaumann R., Williams D. A., Buczkowski D. L., Yingst R. A., Preusker F., Hiesinger H., Schmedemann N., Kneissl T., Vincent J. B., Blewett D. T., Buratti B. J., Carsenty U., Denevi B. W., De Sanctis M. C., Garry W. B., Keller H. U., Kernten E., Krohn K., Li J.-Y., Marchi S., Matz K. D., McCord T. B., McSween H. Y., Mest S. C., Mittlefehldt D. W., Mottola S., Nathues A., Neukum G., O'Brien D. P., Pieters C. M., Prettyman T. H., Raymond

C. A., Roatsch T., Russell C. T., Schenk P., Schmidt B. E., Scholten F., Stephan L., Sykes M. V., Tricarico P., Wagner R., Zuber M. T., and Sierks H. 2012. Vesta's shape and morphology. *Science* 336:687–694, doi:10.1126/science.1219122.

Jouglet D., Poulet F., Milliken R. E., Mustard J. F., Bibring J.-P., Langevin Y., Gondet B., and Gomez C. 2007. Hydration state of the Martian surface as seen by Mars Express OMEGA: 1. Analysis of the 3 μm hydration feature. *Journal of Geophysical Research* 112:E8, doi:10.1029/2006JE002846.

Keil K. 2002. Geological history of asteroid 4 Vesta: The "smallest terrestrial planet." In *Asteroids III*, edited by Bottke W., Cellino A., Paolicchi P., and Binzel R. P. Tucson, Arizona: University of Arizona Press. pp. 573–584.

Larson H. P. and Fink U. 1975. Infrared spectral observations of asteroid 4 Vesta. *Icarus* 26:420–427.

Lazzaro D., Michtchenko T., Carvano J. M., Binzel R. P., Bus S. J., Burbine T. H., Mothe-Dinz T., Florczak M., Angeli C. A., and Harris A. W. 2000. Discovery of a basaltic asteroid in the outer main belt. *Science* 288:2033–2035.

Li J.-Y., McFadden L. A., Thomas P. C., Mutchler M. J., Parker J. W., Young E. F., Russell C. T., Sykes M. V., and Schmidt B. E. 2010. Photometric mapping of Asteroid (4) Vesta's southern hemisphere with Hubble Space Telescope. *Icarus* 208:238–251.

Li J.-Y., Buratti B. J., Capaccioni F., Capria M. T., Le Corre L., Denevi B. W., De Sanctis M. C., Hoffmann M., Hicks M. D., Jorda L., Keller H. U., Mastrodemos N., Mottola S., Nathues A., Pieters C. M., Reddy V., Raymond C. A., Roatsch T., Russell C. T., Schröde S. E., Sykes M. V., and Titus T. 2012. Photometric properties of Vesta. *Asteroids, Comets, Meteors 2012, Proceedings of the conference held May 16-20, 2012 in Niigata, Japan, id. 6387*.

Marchi S., De Sanctis M. C., Lazzarin M., and Magrin S. 2010. On the puzzle of space weathering alteration of basaltic asteroids. *The Astrophysical Journal Letters* 721: L172–L176.

Marchi S., McSween H. Y., O'Brien D. P., Schenk P., De Sanctis M. C., Gaskell R., Jaumann R., Mottola S., Preusker F., Raymond C. A., and Russell C. T. 2012. The violent collisional history of asteroid 4 Vesta. *Science* 336:690–694, doi:10.1126/science.1218757.

Marzari F., Cellino A., and Davis D. R. 1996. Origin and evolution of the Vesta asteroid family. *Astronomy & Astrophysics* 316:248–262.

Mayne R. G., Sunshine J. M., McSween H. Y., Bus S. J., and McCoy T. J. 2011. The origin of Vesta's crust: Insights from spectroscopy of the Vestoids. *Icarus* 214:147–160.

McCord T. B., Adams J. B., and Johnson T. V. 1970. Asteroid Vesta: Spectral reflectivity and compositional implications. *Science* 168:1445–1447.

McCord T. B., Taylor L. A., Combe J.-P., Kramer G., Pieters C. M., Sunshine J. M., and Clark R. N. 2011. Sources and physical processes responsible for OH/H2O in the lunar soil as revealed by the Moon Mineralogy Mapper (M3). *Journal of Geophysical Research* 116, doi:10.1029/2010JE003711.

McCord T. B., Li J.-Y., Combe J.-P., McSween H. Y., Jaumann R., Reddy V., Tosi F., Williams D., Blewett D. T., Turrini N. D., Palomba E., Pieters C. M., De Sanctis M. C., Ammannito E., Capria M. T., Le Corre L., Longobardo A., Nathues A., Mittlefehldt D. W., Schroder S. E., Hiesinger H., Beck A. W., Capaccioni F., Carsenty U., Keller H. U., Denevi B. W., Sunshine J. M., Raymond C. A., and Russell C. T. 2012a. Dark material on Vesta from the infall of carbonaceous volatile-rich material. *Nature* 491:83–86, doi:10.1038/nature11561.

McCord T. B., Combe J.-P., Jaumann R., Palomba E., Reddy V., Blewett D. T., McSween H. Y., Raymond C. A., and Williams D., Dawn Team. 2012b. Dark material on Vesta: Synthesis and interpretations from Dawn observations (abstract #135). 43rd Lunar and Planetary Science Conference. CD-ROM.

McFadden L. A., McCord T. B., and Pieters C. 1977. Vesta: The first pyroxene band from new spectroscopic measurements. *Icarus* 31:439–446.

McSween H. Y., Mittlefehdlt D. W., Beck A. W., Mayne R. G., and McCoy T. J. 2011. HED meteorites and their relationship to the geology of Vesta. *Space Science Reviews* 163:141–174, doi:10.1007/s11214-010-9637-z.

McSween H. Y., Ammannito E., Reddy V., Prettyman T. H., Beck A. W., De Sanctis M. C., Nathues A., Le Corre L., O'Brien D. P., Yamashita N., McCoy T. J., Mittlefehldt D. W., Toplis M. J., Schenk P., Palomba E., Tosi F., Zambon F., Longobardo A., Capaccioni F., Raymond C. A., and Russell C. T. 2013a. Composition of the Rheasilvia basin, a window into Vesta's interior. *Journal of Geophysical Research* 118:335–346, doi:10.1002/jgre.20057.

McSween H. Y., Binzel R. P., De Sanctis M. C., Ammannito E., Prettyman T. H., Beck A. W., Reddy V., Le Corre L., Gaffey M. J., Raymond C. A., and Russell C. T., and the Dawn Science Team. 2013b. Dawn, the Vesta-HED connection, and the geologic context for eucrites, diogenites, and howardites. *Meteoritics & Planetary Science*, doi:10.1111/maps.12108.

Milliken R. E., Mustard J. F., Poulet F., Jouglet D., Bibring J.-P., Gondet B., and Langevin Y. 2007. Hydration state of the Martian surface as seen by Mars Express OMEGA: 2. H2O content of the surface. *Journal of Geophysical Research* 112, E08S07, doi:10.1029/2006JE002853.

Mittlefehldt D. W. 1994. The genesis of diogenites and HED parent body petrogenesis. *Geochimica et Cosmochimica Acta* 58:1537–1552.

Mittlefehldt D. W. 2005. Ibitira: A basaltic achondrite from a distinct parent asteroid and implications for the Dawn mission. *Meteoritics & Planetary Science* 40:665–677.

Mittlefehldt D. W., Li J.-Y., Pieters C. M., de Sanctis M. C., Schroder S. E., Hiesinger H., Blewett D. T., Russell C. T., Raymond C. A., Yingst R. A., and the Dawn Science Team. 2012. Types and distribution of bright materials on 4 Vesta (abstract #1659). 43rd Lunar and Planetary Science Conference. CD-ROM.

Moskovitz N. A., Willman M., Burbine T. H., Binzel R. P., and Bus S. J. 2010. A spectroscopic comparison of HED meteorites and V-type asteroids in the inner Main Belt. *Icarus* 208:773–788.

Nyquist L. E., Reese Y., Weismann H., Shih C.-Y., and Takeda H. 2003. Fossil ^{26}Al and ^{53}Mn in the asuka 881394 eucrite: Evidence of the earliest crust on asteroid 4 Vesta. *Earth and Planetary Science Letters* 214:11.

Palomba E., Combe J.-P., McCord T. B., De Sanctis M. C., Ammannito E., Longobardo A., Tosi F., Capaccioni F.,

Blewett D. T., Jaumann R., McSween H., Raymond C. A., Reddy V., Williams D., Russell C. T., and the Dawn Team. 2012. Composition and mineralogy of dark material deposits on Vesta (abstract #1930). 43rd Lunar and Planetary Science Conference. CD-ROM.

Pieters C. M., Goswami J. N., Clark R. N., Annadurai M., Boardman J., Buratti B., Combe J.-P., Dyar M. D., Green R., Head J. W., Hibbitts C., Hicks M., Isaacson P., Klima R., Kramer G., Kumar S., Livo E., Lundeen S., Malaret E., McCord T., Mustard J., Nettles J., Petro N., Runyon C., Staid M., Sunshine J., Taylor L. A., Tompkins S., and Varanasi P. 2009. Character and spatial distribution of OH/H2O on the surface of the Moon seen by M3 on Chandrayaan-1. *Science* 326:568–572, doi: 10.1126/science.1178658.

Pieters C. M., Ammannito E., Blewett D. T., Denevi B. W., De Sanctis M. C., Gaffey M. J., Le Corre L., Li J.-Y., Marchi S., McCord T. B., McFadden L. A., Mittlefehldt D. W., Nathues A., Palmer E., Reddy V., Raymond C. A., and Russell C. T. 2012. The distinctive space weathering on Vesta. *Nature* 491:79–82, doi:10.1038/nature11534.

Prettyman T. H., Mittlefehldt D. W., Yamashita N., Lawrence D. J., Beck A. W., Feldman W. C., McCoy T. J., McSween H. Y., Toplis M. J., Titus T. N., Tricarico P., Reedy R. C., Hendricks J. S., Forni O., Le Corre L., Li J.-Y., Mizzon H., Reddy V., Raymond C. A., and Russell C. T. 2012. Elemental mapping by Dawn reveals exogenic H in Vesta's regolith. *Science* 338:242–246.

Reininger F., Coradini A., Cappaccioni F., Capria M., Cerroni P., De Sanctis M., Magni G., Drossart P., Barucci M., Bockelee-Morvan D., Combes M., Crovisier J., Encrenaz T., Reess J., Semery A., Tiphene D., Arnold G., Carsenty U., Michaelis H., Mottola S., Neukum G., Peter G., Schade U., and the VIRTIS CoI team. 1996. VIRTIS: Visible Infrared Thermal Imaging Spectrometer for the Rosetta mission. *SPIE* 2819:66–77, doi:10.1117/12.258082.

Righter K. and Drake M. J. 1997. A magma ocean on Vesta: Core formation and petrogenesis of eucrites and diogenites. *Meteoritics & Planetary Science* 32:929–944.

Rivkin A. S., Howell E. S., Vilas F., and Lebofsky L. A. 2002. Hydrated minerals on asteroids: The astronomical record. In *Asteroids III*, edited by Bottke W., Cellino A., Paolicchi P., and Binzel R. P. Tucson, Arizona: University of Arizona Press. pp. 235–253.

Rivkin A. S., McFadden L. A., Binzel R. P., and Sykes M. 2006. Rotationally-resolved spectroscopy of Vesta I: 2 4 μm region. *Icarus* 180:464–472, doi:10.1016/j.icarus.2005.09.012.

Russell C. T., Raymond C. A., Coradini A., McSween H. Y., Zuber M. T., Nathues A., De Sanctis M. C., Jaumann R., Konopliv A. S., Preusker F., Asmar S. W., Park R. S., Gaskell R., Keller H. U., Mottola S., Roatsch T., Scully J. E. C., Smith D. E., Tricarico P., Toplis M. J., Christensen U. R., Feldman W. C., Lawrence D. J., McCoy T. J., Prettyman T. H., Reedy R. C., Sykes M. E., and Titus T. N. 2012. Dawn at Vesta: Testing the protoplanetary paradigm. *Science* 336:684–686, doi:10.1126/science.1219381.

Schiller M., Baker J., Creech J., Paton C., Millet M.-A., Irving A., and Bizzarro M. 2011. Rapid timescales for magma ocean crystallization on the howardite-eucrite-diogenite parent body. *The Astrophysical Journal Letters* 740:L22, doi:10.1088/2041-8205/740/1/L22.

Schroder S. E., Li J.-Y., Mittlefehldt D. W., Pieters C. M., de Sanctis M. C., Hiesinger H., Blewett D. T., Russell C. T., Raymond C. A., and Keller H. U. 2012. Visible color and photometry of bright materials on Vesta (abstract #2459). 43rd Lunar and Planetary Science Conference. CD-ROM.

Scott E. R. D., Greenwood R. C., Franchi I. A., and Sanders I. S. 2009. Oxygen isotopic constraints on the origin and parent bodies of eucrites, diogenites, and howardites. *Geochimica et Cosmochimica Acta* 73:5835–5853.

Shearer C. K., Fowler G. W., and Papike J. J. 1997. Petrogenetic models for magmatism on the eucrite parent body: Evidence from orthopyroxene in diogenites. *Meteoritics & Planetary Science* 32:877–889.

Shkuratov Y., Starukhina L., Hoffmann H., and Arnold G. 1999. A model of spectral albedo of particulate surfaces: Implications for optical properties of the moon. *Icarus* 137:235–246.

Sierks H., Keller H. U., Jaumann R., Michalik H., Behnke T., Bubenhagen F., Büttner I., Carsenty U., Christensen U., Enge R., Fiethe B., Gutiérrez Marqués P., Hartwig H., Krüger H., Kühne W., Maue T., Mottola S., Nathues A., Reiche K.-U., Richards M. L., Roatsch T., Schröder S. E., Szemerey I., Tschentscher M., and Tschentscher M. 2011. The Dawn framing camera. *Space Science Reviews* 163:263–327.

Sunshine J. M., Farnham T. L., Feaga L. M., Groussin O., Merlin F., Milliken R. E., and A'Hearn M. F. 2009. Temporal and spatial variability of lunar hydration as observed by the deep Impact spacecraft. *Science* 326:565–568, doi: 10.1126/science.1179788.

Thomas P. C., Binzel R. P., Gaffey M. J., Storrs A. D., Wells E. N., and Zellner B. H. 1997. Impact excavation on asteroid 4 Vesta: Hubble Space Telescope results. *Science* 277:1492–1495.

Treiman A. H., Morris R. V., Kring D. A., Mittlefehldt D. W., and Jones J. H. 2008. Petrography and origin of the unique achondrite GRA 06128 & 06129: Preliminary results (abstract #2215). 38th Lunar and Planetary Science Conference. CD-ROM.

Vernazza P., Mothe-Diniz T., Barucci M. A., Birlan M., Carvano J. M., Strazzulla G., Fulchignoni M., and Migliorini A. 2005. Analysis of near-IR spectra of 1 Ceres and 4 Vesta, targets of the Dawn mission. *Astronomy & Astrophysics* 436:1113–1121.

Vernazza P., Brunetto R., Strazzulla G., Fulchignoni M., Rochette P., Meyer-Vernet N., and Zouganelis I. 2006. Asteroid colors: A novel tool for magnetic field detection? The case of Vesta. *Astronomy & Astrophysics* 451:L43–L46.

Veverka J., Squyres S. W., Thomas P., Simonelli D., and Morrison D. 1980. Photometric studies of the satellites of Jupiter using Voyager imaging data. In *Reports of planetary geology program* 1979–1980, edited by Wirth P., Greeley R., Dalli R. Wshington, D.C.: NASA. pp. 336–337.

Veverka J., Robinson M., Thomas P., Murchie S., Bell J. F., III, Izenberg N., Chapman C., Harch A., Bell M., Carcich B., Cheng A., Clark B., Domingue D., Dunham D., Farquhar R., Gaffey M. J., Hawkins E., Joseph J., Kirk R., Li H., Lucey P., Malin M., Martin P., McFadden L., Merline W. J., Miller J. K., Owen W. M., Jr., Peterson C., Prockter L., Warren J., Wellnitz D., Williams B. G., Yeomans D. K., and Yeomans D.

K. 2000. NEAR at Eros: Imaging and spectral results. *Science* 289:2088–2097, doi:10.1126/science.289.5487.2088.

Warren P. H. 1997. Magnesium oxide iron oxide mass balance constraints and a more detailed model for the relationship between eucrites and diogenites. *Meteoritics & Planetary Science* 32:945–963.

Xu S., Binzel R. P., Burbine T. H., and Bus S. J. 1995. Small main-belt asteroid spectroscopic survey: Initial results. *Icarus* 115:1–35.